

IEEE Copyright Notice

This work has been submitted to the IEEE for possible publication. Copyright may be transferred without notice, after which this version may no longer be accessible.

Accurate Open-Loop Control of a Soft Continuum Robot Through Visually Learned Latent Representations

Henrik Krauss¹, Johann Licher², Naoya Takeishi³, Annika Raatz², Takehisa Yairi³

Abstract—This work addresses open-loop control of a soft continuum robot (SCR) from video-learned latent dynamics. Visual Oscillator Networks (VONs) from previous work are used, that provide mechanistically interpretable 2D oscillator latents through an attention broadcast decoder (ABCD). Open-loop, single-shooting optimal control is performed in latent space to track image-specified waypoints without camera feedback. An interactive SCR live simulator enables design of static, dynamic, and extrapolated targets and maps them to model-specific latent waypoints. On a two-segment pneumatic SCR, Koopman, MLP, and oscillator dynamics, each with and without ABCD, are evaluated on setpoint and dynamic trajectories. ABCD-based models consistently reduce image-space tracking error. The VON and ABCD-based Koopman models attain the lowest MSEs. Using an ablation study, we demonstrate that several architecture choices and training settings contribute to the open-loop control performance. Simulation stress tests further confirm static holding, stable extrapolated equilibria, and plausible relaxation to the rest state. To the best of our knowledge, this is the first demonstration that interpretable, video-learned latent dynamics enable reliable long-horizon open-loop control of an SCR.

I. INTRODUCTION

Recent developments in data-driven methods have enabled discovery of latent dynamics in high-dimensional data, such as video. Prominent methods are Koopman theory, (extended) dynamic mode decomposition (DMD) and spectral submanifolds (SSMs) [1]–[4].

Soft continuum robots (SCR) exhibit continuous deformation and a theoretically infinite degree of freedom and are therefore challenging to model and control [5]. Classical SCR modelling approaches, such as piece-wise constant curvature (PCC) or Cosserat rod-based dynamics, require manual model derivation and are either limited in accuracy or computational efficiency [6]. Hybrid approaches have been proposed to overcome these limitations [7]. Licher et al. have achieved highly accurate closed-loop dynamic control of an SCR based on nonlinear evolutionary model-predictive

This work was supported in part by JST PRESTO under Grant JP-MJPR24T6, in part by JSPS KAKENHI under Grant JP25H01454, and in part by the Deutsche Forschungsgemeinschaft (DFG, German Research Foundation) under Grant No. 405030609.

¹Henrik Krauss is with Department of Advanced Interdisciplinary Studies, The University of Tokyo, Tokyo, 153-8904, Japan. henrik1.krauss@gmail.com

²Johann Licher and Annika Raatz are with the Institute of Assembly Technology and Robotics, Leibniz University Hannover, 30823 Germany. licher@match.uni-hannover.de

³Naoya Takeishi and Takehisa Yairi are with the Research Center for Advanced Science and Technology, The University of Tokyo, Tokyo, 153-8904, Japan.

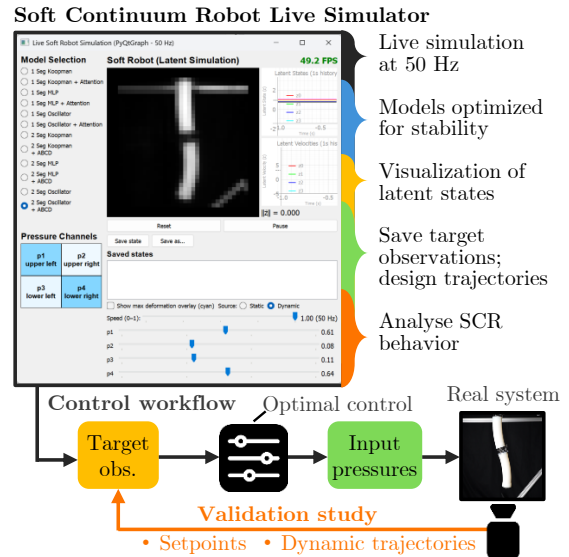


Fig. 1: Overview of this study’s approach: an SCR live simulator is employed to generate target states for open-loop optimal control of the physical SCR. The feasibility of this method is validated across diverse trajectories.

control (MPC) applied to a physics-informed neural network (PINN) based on Cosserat rod dynamics [8].

In contrast to enabling fast solution of computationally expensive, manually derived models, recent developments also focused on deriving low-order representations that describe the complex nonlinear dynamics of SCRs. Examples include low-dimensional strain parameterizations [9], or low-order finite-element models which have been applied to optimal control [10]. Furthermore, Koopman theory and SSMs have been used for accurate closed-loop control of SCRs [11], [12]. As part of fully data-driven approaches, Stölzle et al. have introduced coupled oscillator networks (CONs) that learn latent models of soft robots from video, and applied it to control of a simulated SCR [13].

While easily derived from data, they lack mechanistic interpretability and proof of generalization. In our previous work we presented visual oscillator networks (VONs), coupling ABCD attention maps with 2D oscillator positions for on-image interpretable dynamics [14] that generalize well and show good prediction performance.

However, latent dynamical models are *rarely used open-loop* because prediction errors accumulate over time and can drive the trajectory off the manifold on which the real system

dynamics are represented. Some studies have demonstrated open-loop latent dynamical controllers for soft actuators, e.g. by learning inverse models from actuator responses and iterative learning control data [15] or by training a recurrent neural network to predict images from actuation inputs and using it to optimize inputs for trajectory tracking [16].

While recent work has demonstrated open-loop control of SCRs using video-learned recurrent models, these rely on image-level, global optimization to maintain performance, show limited accuracy, and lack evidence of structural stability. To the best of our knowledge, no study has shown that explicit latent dynamical models can support stable and accurate long-horizon open-loop control of soft continuum robots without camera feedback. Moreover, in real scenarios, full-state feedback is often limited, and fully relying on reproducible, external vision limits application. Further, targets may need to come from unseen images, derived artificially from user input (e.g. by drawing [16], [17]) or simulation.

This work addresses three key challenges in learning-based control of SCRs: (i) the lack of interpretability of learned representations for control, (ii) reliable open-loop control without feedback, and (iii) the availability of target states, including unseen or extrapolated configurations. Our main contributions are:

- 1) We present the first demonstration of accurate and reliable open-loop optimal control of an SCR using explicit latent dynamics models learned from visual observations without prior manual modeling of system dynamics. This is enabled by mechanistically interpretable models, specifically VONs with the ABCD. We evaluate VONs on the real system and against baselines (Fig. 1), analyze limitations in simulation, and provide training guidelines via an ablation study.
- 2) We introduce an SCR live simulator for interactive target state and trajectory design, supporting control with unseen or extrapolated targets (Fig. 1).

II. METHODS

A. Learning Latent Dynamics from Video

We learn latent dynamical models from video using an encoder–dynamics–decoder model based on [2], [13]. For an image $\mathbf{o}^{(i)}$ at step i , the encoder φ produces latent coordinates

$$\mathbf{z}^{(i)} = \varphi(\mathbf{o}^{(i)}), \quad (1)$$

and the dynamics model f_{dyn} predicts the next latent coordinates and velocities under input $\mathbf{u}^{(i)}$,

$$(\hat{\mathbf{z}}^{(i+1)}, \hat{\dot{\mathbf{z}}}^{(i+1)}) = f_{\text{dyn}}(\mathbf{z}^{(i)}, \dot{\mathbf{z}}^{(i)}, \mathbf{u}^{(i)}), \quad (2)$$

which is decoded to the next image $\hat{\mathbf{o}}^{(i+1)} = \varphi^{-1}(\hat{\mathbf{z}}^{(i+1)})$.

Following [13], we define the full latent state as $\boldsymbol{\xi}^{(i)} = [\mathbf{z}^{(i)\top}, \dot{\mathbf{z}}^{(i)\top}]^\top$. The latent velocity is obtained from the encoder Jacobian,

$$\dot{\mathbf{z}}^{(i)} = \frac{\partial \varphi}{\partial \mathbf{o}}(\mathbf{o}^{(i)}) \dot{\mathbf{o}}^{(i)}, \quad (3)$$

and central finite differences of observations. We use a β -VAE [18] and train end-to-end with static and dynamic image

reconstruction, and latent consistency losses, originally based on [2] and similar to [14].

Three latent dynamical models are compared, where for all $\mathbf{B}(\cdot)$ is parameterized by a multi-layer perceptron (MLP):

(I) *Koopman*: We use a transition matrix \mathbf{A} for the latent-state update

$$\boldsymbol{\xi}^{(i+1)} = \mathbf{A}\boldsymbol{\xi}^{(i)} + \mathbf{B}(\mathbf{u}^{(i)}). \quad (4)$$

(II) *MLP*: Providing a flexible baseline, an MLP predicts the next latent velocity as

$$\dot{\mathbf{z}}^{(i+1)} = f_{\text{MLP}}(\boldsymbol{\xi}^{(i)}) + \mathbf{B}(\mathbf{u}^{(i)}), \quad (5)$$

from which the next latent coordinate

$$\mathbf{z}^{(i+1)} = \mathbf{z}^{(i)} + \Delta t \dot{\mathbf{z}}^{(i+1)}. \quad (6)$$

is obtained from integration to ensure kinematic consistency.

(III) *Oscillator network*: The latent coordinates follow the equation of motion

$$\mathbf{M}\ddot{\mathbf{z}} + \mathbf{D}\dot{\mathbf{z}} + \mathbf{K}(\mathbf{z} - \mathbf{z}_0) = \mathbf{B}(\mathbf{u}), \quad (7)$$

where \mathbf{z}_0 is an optional, learnable non-zero rest position used by VONs, and \mathbf{M} , \mathbf{D} , \mathbf{K} denote mass, damping, and stiffness matrices. We integrate this system using a symplectic Euler scheme with implicit damping:

$$\dot{\mathbf{z}}^{(i+1)} = \boldsymbol{\Gamma}^{-1} \left[\dot{\mathbf{z}}^{(i)} + \Delta t \mathbf{M}^{-1} \left(\mathbf{B}(\mathbf{u}^{(i)}) - \mathbf{K}(\mathbf{z}^{(i)} - \mathbf{z}_0) \right) \right], \quad (8)$$

$$\mathbf{z}^{(i+1)} = \mathbf{z}^{(i)} + \Delta t \dot{\mathbf{z}}^{(i+1)}, \quad (9)$$

with $\boldsymbol{\Gamma} = \text{diag}(\mathbf{I} + \Delta t \mathbf{M}^{-1} \mathbf{D})$.

Apart from the newly introduced implicit damping, the Koopman and oscillator formulations are consistent with our previous work. All three models, including the MLP, can be combined with the ABCD introduced in [14]. In particular, the oscillator model with the attention coupling loss, aligning the relative movements of latent 2D oscillators with corresponding ABCD attention maps yields the VON.

To improve suitability for open-loop control and extending on [14], we further replace the dynamic single-step losses by multi-step losses over an H -step rollout, where H increases over training epochs, for the latent dynamical consistency loss

$$\mathcal{L}_d^{(H)} = \frac{1}{N} \sum_{n=1}^N \frac{1}{H} \sum_{h=1}^H \text{MSE}(\varphi^{-1}(\hat{\mathbf{z}}^{(n,h)}), \mathbf{o}^{(n,h)}), \quad (10)$$

as well as the dynamic reconstruction loss

$$\begin{aligned} \mathcal{L}_z^{(H)} = \frac{1}{N} \sum_{n=1}^N \frac{1}{H} \sum_{h=1}^H & \left(\text{MSE}(\hat{\mathbf{z}}^{(n,h)}, \mathbf{z}^{(n,h)}) \right. \\ & \left. + \text{MSE}(\Delta t \cdot \hat{\dot{\mathbf{z}}}^{(n,h)}, \Delta t \cdot \dot{\mathbf{z}}^{(n,h)}) \right). \end{aligned} \quad (11)$$

Here (n, h) denotes the h -th step of the n -th sequence in the batch of size N . For all model types, we additionally use an

adjusted, simplified rest-state loss (instead of a steady-state loss)

$$\mathcal{L}_s = \frac{1}{2} \left(\text{MSE}(\varphi(\mathbf{o}_{\text{rest}}), \mathbf{z}_0) + \left(\text{MSE}([f_{\text{dyn}}(\varphi(\mathbf{o}_{\text{rest}}), \mathbf{0}, \mathbf{u}_{\text{rest}})]_1, \mathbf{z}_0) + \text{MSE}(\Delta t \cdot [f_{\text{dyn}}(\varphi(\mathbf{o}_{\text{rest}}), \mathbf{0}, \mathbf{u}_{\text{rest}})]_2, \mathbf{0}) \right) \right), \quad (12)$$

enforcing that rest-state \mathbf{o}_{rest} encodes to \mathbf{z}_0 and stays at equilibrium under rest actuation \mathbf{u}_{rest} . The rest state is also the starting point for control from rest. Finally, for VONs we apply mean correction in the KL term,

$$\mathcal{L}_{\text{KL}}^{(z_0)} = \frac{-1}{2N} \sum_{i=1}^N \sum_j \left(1 + \log(\sigma_j^{(i)})^2 - (\mu_j^{(i)} - z_{0,j})^2 - (\sigma_j^{(i)})^2 \right), \quad (13)$$

where j refers to the j -th latent dimension of $\mathbf{z}^{(i)}$.

B. Predictive Control in Latent Space

We use a discrete-time formulation with step index $i = 0, \dots, T-1$ at 50 Hz. Given an initial latent state $(\mathbf{z}^{(0)}, \dot{\mathbf{z}}^{(0)})$ and a horizon of T steps, we solve a single-shooting open-loop optimal control problem over the control sequence $\mathbf{u}^{(0)}, \dots, \mathbf{u}^{(T-1)}$ subject to the learned latent dynamics

$$(\mathbf{z}^{(i+1)}, \dot{\mathbf{z}}^{(i+1)}) = f_{\text{dyn}}(\mathbf{z}^{(i)}, \dot{\mathbf{z}}^{(i)}, \mathbf{u}^{(i)}), \quad i = 0, \dots, T-1, \quad (14)$$

with $(\mathbf{z}^{(T)}, \dot{\mathbf{z}}^{(T)})$ being the terminal state.

Targets are one or more observations $\{\mathbf{o}_k^*\}_{k=1}^K$. Latent targets are $\mathbf{z}_k^* = \varphi(\mathbf{o}_k^*)$; $\dot{\mathbf{z}}_k^*$ is from central finite differences via (3) when available, else $\mathbf{0}$ for static and final targets. For $K > 1$, the target points are distributed uniformly over the horizon at state indices τ_1, \dots, τ_K with $\tau_1 = 1$, $\tau_K = T$, e.g. $\tau_k = 1 + \text{round}((k-1)(T-1)/(K-1))$, and the active target index $k(i)$ is chosen as one of two options, as either the next or closest target from current state index i :

$$k(i) = \begin{cases} \min\{k \in \{1, \dots, K\} \mid \tau_k \geq i\}, & \text{(next target)} \\ \arg \min_{k \in \{1, \dots, K\}} |i - \tau_k|, & \text{(closest target)}. \end{cases} \quad (15)$$

With $(\bar{\mathbf{z}}^{(i)}, \bar{\dot{\mathbf{z}}}^{(i)}) = (\mathbf{z}_{k(i)}^*, \dot{\mathbf{z}}_{k(i)}^*)$, we solve the optimal control problem

$$\begin{aligned} \min_{\mathbf{u}^{(0:T-1)}} J = & \underbrace{\frac{w_Q}{T} \sum_{i=1}^T \|\mathbf{z}^{(i)} - \bar{\mathbf{z}}^{(i)}\|_2^2 + \frac{w_{\dot{Q}}}{T} \sum_{i=1}^T \|\dot{\mathbf{z}}^{(i)} - \bar{\dot{\mathbf{z}}}^{(i)}\|_2^2}_{\text{cost to next or closest waypoint}} \\ & + \underbrace{\frac{w_{Q_k}}{K} \sum_{k=1}^K \|\mathbf{z}^{(\tau_k)} - \mathbf{z}_k^*\|_2^2 + \frac{w_{\dot{Q}_k}}{K} \sum_{k=1}^K \|\dot{\mathbf{z}}^{(\tau_k)} - \dot{\mathbf{z}}_k^*\|_2^2}_{\text{waypoint-exact cost}} \\ & + \underbrace{w_{Q_f} \|\mathbf{z}^{(T)} - \bar{\mathbf{z}}^{(T)}\|_2^2 + w_{\dot{Q}_f} \|\dot{\mathbf{z}}^{(T)} - \bar{\dot{\mathbf{z}}}^{(T)}\|_2^2}_{\text{terminal cost}} \\ & + \frac{w_R}{T-1} \sum_{i=1}^{T-1} \|\Delta \mathbf{u}^{(i)}\|_2^2 + \frac{w_{\Delta u}}{T-1} \sum_{i=1}^{T-1} \phi(\Delta \mathbf{u}^{(i)}), \end{aligned} \quad (16)$$

where w_Q and $w_{\dot{Q}}$ penalize latent state tracking errors along the trajectory to the next or closest waypoint, w_{Q_k} and $w_{\dot{Q}_k}$ penalize the error at each waypoint τ_k , w_{Q_f} and $w_{\dot{Q}_f}$ penalize terminal errors at step T , w_R penalizes step-wise control increments $\Delta \mathbf{u}^{(i)} = \mathbf{u}^{(i)} - \mathbf{u}^{(i-1)}$ for $i = 1, \dots, T-1$, and $w_{\Delta u}$ penalizes only increments exceeding a prescribed bound after

$$\phi(\Delta \mathbf{u}) = \|\max(|\Delta \mathbf{u}| - \Delta \mathbf{u}_{\text{max}}, \mathbf{0})\|_2^2. \quad (17)$$

where the absolute value and max operator are applied element-wise, to further respect limits of the SCR pressure controller.

In practice, state and velocity errors in the cost are scaled by the mean per-dimension standard deviation of latents on validation data, so loss weights are comparable across models and relative structure is preserved. The rollout is initialized with $\mathbf{u}^{(0)}$ corresponding to $(\mathbf{z}^{(0)}, \dot{\mathbf{z}}^{(0)})$ (static SCR configuration fixes chamber pressures); $\mathbf{u}^{(1)}, \dots, \mathbf{u}^{(T-1)}$ are optimized by gradient descent through the latent rollout.

C. Obtaining Target Observations Through an SCR Live Simulator

We present an SCR live simulator in Fig. 1, built on Python and PyQtGraph that shows the SCR as predicted by Koopman, MLP, and oscillator models with or without ABCD under user input. Pressure sliders and controls allow interactive design of static, dynamic, and extrapolated targets in image space. Pressures outside the dataset range yield unseen targets and can test extrapolation of the learned models. Saved states store decoded observations and applied input, so target latent states and velocities can be derived per model. The live simulator will be made available in a code repository¹.

III. EXPERIMENTS

A. Hardware, Dataset, and Training of Models

We use a two-segment SCR with three pressure chambers per segment. Two chambers per segment are pressurized equally, providing four effective inputs and planar motion perpendicular to the camera axis. Further details on the dimensions and manufacturing of the actuator are given in [19]. The dataset is a modified version of [14], with two 15-minute recordings at 50 Hz (pressures down-sampled to this rate). The first uses smooth sinusoidal excitations and linear interpolation over 0 kPa to 86 kPa (extended to lower pressures than the prior version), the second uses step excitations. Both were captured with a fixed industrial camera for repeatable validation. The dataset is released as v2². Models are trained only on the sinusoidal excitations dataset, with the step dataset reserved for validation. We train six main models for control evaluation, namely Koopman, MLP, and Oscillator networks, each in plain form and with the ABCD decoder. The oscillator network with ABCD is the VON. Seven ablation VONs are also trained to assess the

¹github.com/UThenrik/visual_oscillators_for_SCR

²<https://zenodo.org/records/17812071>

impact of architecture and hyperparameter choices on open-loop control performance. Training code and configurations, building on [14] are provided in the same code repository as the live simulator.

B. Open-Loop Control

We evaluate open-loop control for setpoints and dynamic trajectories. Setpoint tasks test rest-to-target, target-to-target and target-to-rest control for previously tested (normal) and slightly extrapolated states; dynamic tasks include tracking multiple waypoints, reaching upswing positions (outside the dataset range), and long-horizon prediction. Target observations are obtained in two ways. *Setpoint Normal* uses frames from the step-validation dataset, encoded per model. All other target observations are designed in the live simulator (Sec. II-C) using the plain Koopman model, and using the VON for the long dynamic trajectories. Table I summarizes the trajectory types and control parameters.

TABLE I: Trajectory types and control parameters. n = number of trajectories tested.

Name	n	T	K	w_Q	$w_{\dot{Q}}$	w_{Q_k}	$w_{\dot{Q}_k}$	w_{Q_f}	$w_{\dot{Q}_f}$
Setp. Normal	9	100	2	1	0.002	0	0	0	0
Setp. Extrap.	6	100	2	1	0.002	0	0	0	0
Dyn. Normal	5	200	8	1	0	0	0	0	0.002
Dyn. Fast	3	150	8	1	0	0	0	0	0.002
Dyn. Upswing	3	150	3	0	0	1	0.002	0	0
Dyn. Long	5	1000	22	1	0	0	0	0	0.002

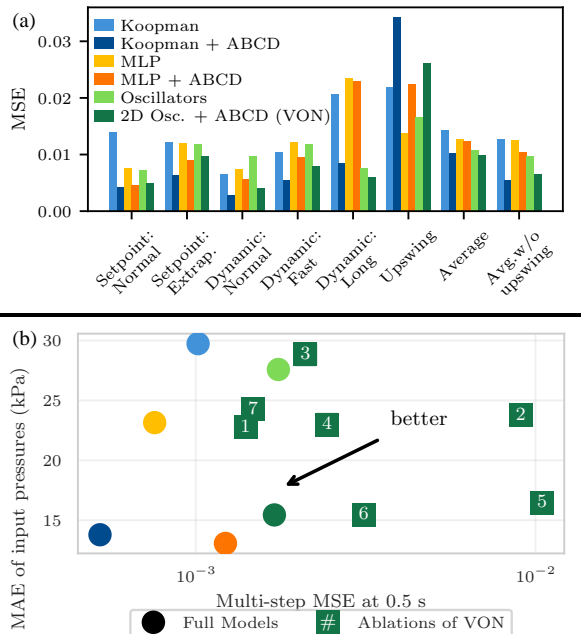


Fig. 2: (a) Model performances in open-loop control over various trajectory types (image MSEs). (b) MAE of input pressure prediction of open-loop setpoint control over multi-step prediction errors (50 samples each), including ablations.

Optimized controls (Sec. III-B) are executed on the real system. MSEs are computed in image space per trajectory

and model over all waypoints except the initial. For setpoints, all post-initial observations are included.

Fig. 2(a) shows the average MSEs for all six models, and Fig. 3(a) gives representative trajectory examples. Models with ABCD decoders consistently outperform their plain counterparts, except for upswing trajectories; the Koopman and oscillator-based ABCD (i.e., VON) models achieve the lowest overall MSEs at 1.03×10^{-2} and 9.80×10^{-3} . Models are trained on measured pressures, so optimization disregards the dynamics of the low-level pressure controller. The higher errors observed for the upswing tasks likely result from the low-level pressure controller being too slow to track pressure changes under fast oscillations, as also evident in Fig. 3(c). In contrast, for the faster dynamic trajectories the required pressure changes are within the controller’s capabilities, the real pressure matches the generated one well, as shown in Fig. 3(b), which shows the latent target and states and predictions corresponding to the same dynamic, fast trajectory depicted in (a). Fig. 2 also gives average MSEs excluding upswing. Using the ABCD consistently reduces open-loop control errors excluding upswing trajectories: for Koopman, the MSE drops from 1.28×10^{-2} to 5.45×10^{-3} ; for MLP, from 1.25×10^{-2} to 1.03×10^{-2} ; and for the Oscillator, from 9.60×10^{-3} to 6.55×10^{-3} . This result highlights the effectiveness of the ABCD decoder.

C. Ablation study

We ablate design choices that enable stable open-loop control [14] to guide video-based latent dynamical modeling for control. We train seven ablation models. In each, exactly one choice is changed from the full VON. The ablation models use: (1) linear excitation B instead of an MLP, (2) loss weights that prioritize dynamic image reconstruction as in [13], [14], (3) VAE $\beta = 0.01$ instead of 0.0001, (4) no rest-state loss, (5) no multi-step loss, (6) Rayleigh damping instead of full damping, (7) symplectic Euler without implicit damping. All other settings in each ablation match the full model.

As an indicator for open-loop setpoint control performance without hardware validation, we use MAE between predicted and real input pressures on 50 setpoints from the step excitation dataset (setpoint optimization as in Sec. III-B). Fig. 2(b) plots this pressure MAE against multi-step image MSE (50 validation trajectories). ABCD-based models yield lower pressure MAE and better multi-step MSE, except for the MLP-based models. Overall best performing is Koopman + ABCD with multi-step MSE of 5.23×10^{-4} and a pressure MAE of 13.79 kPa. Within the VON ablation study, the full model reaches a multi-step MSE of 1.71×10^{-3} and the lowest pressure MAE of 15.44 kPa, versus ablation averages 4.92×10^{-3} and 22.08 kPa. It lies best (lower-left), so we conclude all seven changes contribute to accurate open-loop control. Note that pressure MAE can stay high when image MSE is low for visually similar configurations. A further insightful observation is that low multi-step MSE does not seem to guarantee good open-loop control.

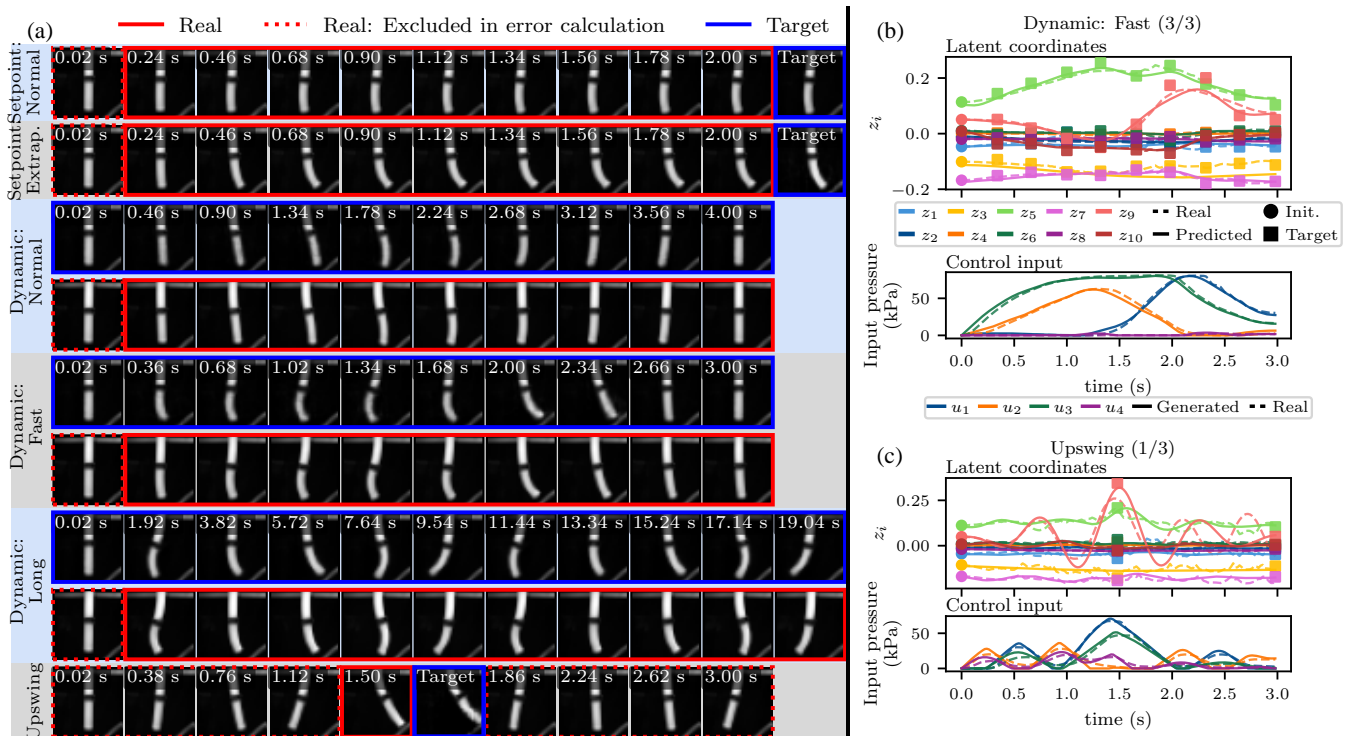


Fig. 3: (a) Examples for trajectories evaluated for open-loop optimal open-loop control. The real trajectories shown are based on the VON model. All target trajectories are accurately achieved, except the upswing, where an additional plot highlights a deviation between set and measured pressure inputs. (b) Predicted and real latent trajectories and input pressures for the fast dynamic trajectory and upswing trajectory (c), depicted on the left.

D. Simulational experiments

Three stress tests shown in Fig. 4 are run in simulation for all six models to assess control-relevant properties. First (a), we assess static holding: for 50 static states from the step excitation dataset, we keep the corresponding chamber pressures constant and run the dynamics for 500 steps or 10 s, measuring the image MSE between the decoded prediction and the initial observation. This tests the models' capability of holding static equilibria. Second (b), we test a pressure ramp-up to pressures outside of the dataset limit, applying a smooth cosine ramp in pressure and then holding the final pressure, again plotting the image MSE over time to assess whether the predicted configuration stays close to the visually designed target under sustained loading. Third (c), we apply cosine excitation within dataset limits, following a release, tracking the MSE to the rest observation. This probes whether the models exhibit a plausible relaxation back towards rest.

The upper row of Fig. 4 shows MSEs over time, while below we can see initial and target observations for (a), final state of the VON model for (b), and rest state for (c). The right column shows the decoded observations at the final simulation step. Across all three tests, ABCD-based models drift less than their plain counterparts. This is especially the case for the Koopman and VONs which provide highly reasonable predictions in the tested scenarios. Fig. 4(b), center, shows VON oscillator and stiffness forces, explaining

stability under extrapolated pressures. Here, excitation forces predominantly push the SCR to the right, while stiffness forces act in opposite direction back to rest position, creating a stable equilibrium.

IV. CONCLUSIONS

We have demonstrated that interpretable, video-learned latent dynamics enable accurate open-loop control of a soft continuum robot (SCR). Using VONs with the custom ABCD decoder, latent states admit on-image visualization and physically meaningful oscillator dynamics. With improved training (multi-step prediction, rest-state consistency, damping), these models allow single-shooting optimal control to track visually specified static and dynamic trajectories on hardware. Target states are obtained from a custom SCR live simulator that maps designed observations to model-specific latent waypoints, addressing open-loop reliability without camera feedback and availability of suitable (including extrapolated) targets. On the real system, ABCD-based models consistently outperform their plain counterparts on various trajectories, and in simulation, they show stable static holding, extrapolated ramp-up, and return to the global equilibrium. Koopman with ABCD attains the strongest performance overall, with the VON second-best. Further, an ablation study gives practical guidance for training such models for control.

Future work should move from open-loop to closed or

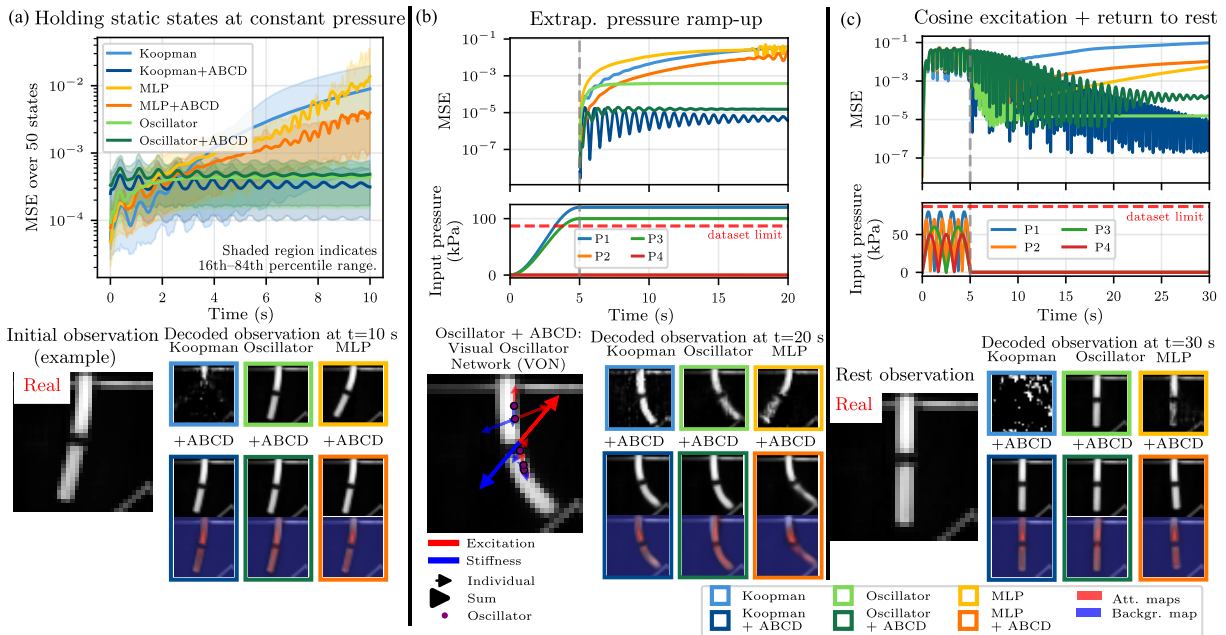


Fig. 4: Simulation results for three stress tests. (a) Static holding at constant pressure for 50 static states. (b) Cosine ramp-up to extrapolated pressures. (c) Cosine excitation within dataset limits followed by a release. The upper row shows image-space MSEs over time. Below are expected final observation in (a) and (c), and (b) visualizes VON oscillator and stiffness forces. The lower-right of each column shows decoded observations at the final simulation step. ABCD-based models provide more stable and reasonable predictions.

partially feedback-stabilized control, e.g. sensor and end-effector feedback in the model learning. Further, future models should account for low-level pressure controller dynamics to overcome current limitations.

REFERENCES

- [1] N. Takeishi, Y. Kawahara, and T. Yairi, "Learning koopman invariant subspaces for dynamic mode decomposition," *Advances in neural information processing systems*, vol. 30, 2017.
- [2] B. Lusch, J. N. Kutz, and S. L. Brunton, "Deep learning for universal linear embeddings of nonlinear dynamics," *Nature communications*, vol. 9, no. 1, p. 4950, 2018.
- [3] S. L. Brunton, M. Budišić, E. Kaiser, and J. N. Kutz, "Modern koopman theory for dynamical systems," *SIAM Review*, vol. 64, no. 2, pp. 229–340, 2022.
- [4] M. Cenedese, J. Axås, B. Bäuerlein, K. Avila, and G. Haller, "Data-driven modeling and prediction of non-linearizable dynamics via spectral submanifolds," *Nature Communications*, vol. 13, no. 1, p. 872, 2022.
- [5] T. G. Thuruthel, Y. Ansari, E. Falotico, and C. Laschi, "Control Strategies for Soft Robotic Manipulators: A Survey," *Soft Robotics*, vol. 5, no. 2, pp. 149–163, 2018.
- [6] C. Armanini, F. Boyer, A. T. Mathew, C. Duriez, and F. Renda, "Soft robots modeling: A structured overview," *IEEE Transactions on Robotics*, vol. 39, no. 3, pp. 1728–1748, 2023.
- [7] E. Falotico, E. Donato, C. Alessi, E. Setti, M. S. Nazeer, C. Agabiti, D. Caradonna, D. Bianchi, F. Piqué, Y. T. Ansari, and M. Killpack, "Learning Controllers for Continuum Soft Manipulators: Impact of Modeling and Looming Challenges," *Advanced Intelligent Systems*, vol. 7, no. 2, p. 2400344, 2025.
- [8] J. Licher, M. Bartholdt, H. Krauss, T.-L. Habich, T. Seel, and M. Schappler, "Adaptive model-predictive control of a soft continuum robot using a physics-informed neural network based on cosserat rod theory," 2025. [Online]. Available: <https://arxiv.org/abs/2508.12681>
- [9] A. Y. Alkayyas, A. T. Mathew, D. Feliu-Talegon, Y. Zweiri, T. G. Thuruthel, and F. Renda, "Structure-preserving model order reduction of slender soft robots via autoencoder-parameterized strain," *IEEE Robotics and Automation Letters*, vol. 10, no. 10, pp. 11 006–11 013, 2025.
- [10] S. Tonkens, J. Lorenzetti, and M. Pavone, "Soft robot optimal control via reduced order finite element models," in *2021 IEEE International Conference on Robotics and Automation (ICRA)*, 2021, pp. 12 010–12 016.
- [11] D. A. Haggerty, M. J. Banks, E. Kamenar, A. B. Cao, P. C. Curtis, I. Mezić, and E. W. Hawkes, "Control of soft robots with inertial dynamics," *Science robotics*, vol. 8, no. 81, p. eadd6864, 2023.
- [12] J. I. Alora, M. Cenedese, G. Haller, and M. Pavone, "Discovering dominant dynamics for nonlinear continuum robot control," *npj Robotics*, vol. 3, no. 1, p. 5, 2025.
- [13] M. Stölzle and C. Della Santina, "Input-to-state stable coupled oscillator networks for closed-form model-based control in latent space," in *Advances in Neural Information Processing Systems*, 2024.
- [14] H. Krauss, J. Licher, N. Takeishi, A. Raatz, and T. Yairi, "Learning visually interpretable oscillator networks for soft continuum robots from video," 2025. [Online]. Available: <https://arxiv.org/abs/2511.18322>
- [15] T. Sugiyama, K. Kutsuzawa, D. Owaki, and M. Hayashibe, "Latent representation-based learning controller for pneumatic and hydraulic dual actuation of pressure-driven soft actuators," *Soft Robotics*, vol. 11, no. 1, pp. 105–117, 2024.
- [16] R. Marques Monteiro, J. Shi, H. Wurdemann, F. Iida, and T. George Thuruthel, "Visuo-dynamic self-modelling of soft robotic systems," *Frontiers in Robotics and AI*, vol. 11, 2024.
- [17] E. Almanzor, F. Ye, J. Shi, T. G. Thuruthel, H. A. Wurdemann, and F. Iida, "Static Shape Control of Soft Continuum Robots Using Deep Visual Inverse Kinematic Models," *IEEE Transactions on Robotics*, vol. 39, no. 4, pp. 2973–2988, 2023.
- [18] I. Higgins, L. Matthey, A. Pal, C. Burgess, X. Glorot, M. Botvinick, S. Mohamed, and A. Lerchner, "beta-vae: Learning basic visual concepts with a constrained variational framework," in *International conference on learning representations*, 2017.
- [19] M. Bartholdt, M. Wiese, M. Schappler, S. Spindeldreier, and A. Raatz, "A Parameter Identification Method for Static Cosserat Rod Models: Application to Soft Material Actuators with Exteroceptive Sensors," in *2021 IEEE/RSJ International Conference on Intelligent Robots and Systems (IROS)*, 2021, pp. 624–631.